

Alma Mater Studiorum Università di Bologna
Archivio istituzionale della ricerca

A comparative structural and spectroscopic study of diiron and diruthenium isocyanide and aminocarbyne complexes

This is the final peer-reviewed author's accepted manuscript (postprint) of the following publication:

Published Version:

Lorenzo Biancalana, Matteo Fiaschi, Gianluca Ciancaleoni, Guido Pampaloni, Valerio Zanotti, Stefano Zacchini, et al. (2022). A comparative structural and spectroscopic study of diiron and diruthenium isocyanide and aminocarbyne complexes. INORGANICA CHIMICA ACTA, 536, 1-9 [10.1016/j.ica.2022.120886].

Availability:

This version is available at: <https://hdl.handle.net/11585/889939> since: 2022-07-04

Published:

DOI: <http://doi.org/10.1016/j.ica.2022.120886>

Terms of use:

Some rights reserved. The terms and conditions for the reuse of this version of the manuscript are specified in the publishing policy. For all terms of use and more information see the publisher's website.

This item was downloaded from IRIS Università di Bologna (<https://cris.unibo.it/>).
When citing, please refer to the published version.

(Article begins on next page)

This is the final peer-reviewed accepted manuscript of:

L. Biancalana, M. Fiaschi, G. Ciancaleoni, G. Pampaloni, V. Zanotti, S. Zacchini, F. Marchetti, "A comparative structural and spectroscopic study of diiron and diruthenium isocyanide and aminocarbyne complexes", *Inorg. Chim. Acta*, **2022**, 536, 120886.

The final published version is available online at:

<https://doi.org/10.1016/j.ica.2022.120886>

Rights / License: Licenza per Accesso Aperto. Creative Commons Attribuzione - Non commerciale - Non opere derivate 4.0 (CCBYNCND)

The terms and conditions for the reuse of this version of the manuscript are specified in the publishing policy. For all terms of use and more information see the publisher's website.

A Comparative Structural and Spectroscopic Study of Diiron and Diruthenium Isocyanide and Aminocarbyne Complexes[†]

Lorenzo Biancalana,^a Matteo Fiaschi,^a Gianluca Ciancaleoni,^a Guido Pampaloni,^a Valerio Zanotti,^b

Stefano Zacchini,^{b,*} Fabio Marchetti^{a,*}

^a University of Pisa, Department of Chemistry and Industrial Chemistry, Via G. Moruzzi 13, I-56124
Pisa, Italy.

^b University of Bologna, Department of Industrial Chemistry “Toso Montanari”, Viale Risorgimento 4,
I-40136 Bologna, Italy.

[†] This work is dedicated to Claudio Pettinari, on occasion of his 58th birthday.

* Authors to whom correspondence should be addressed: stefano.zacchini@unibo.it;
fabio.marchetti1974@unipi.it

Abstract

The chemistry of $[\text{Fe}_2\text{Cp}_2(\text{CO})_4]$ (**1-Fe**; $\text{Cp} = \eta^5\text{-C}_5\text{H}_5$) has been widely investigated, and straightforward carbonyl/isocyanide substitution, followed by isocyanide alkylation, provides access to a variety of aminocarbyne complexes, displaying a rich and versatile reactivity. On the other hand, the parallel chemistry of $[\text{Ru}_2\text{Cp}_2(\text{CO})_4]$ (**1-Ru**) has been much less developed, and relevant structural/bonding aspects scarcely elucidated. We report an IR study on **1-Ru** in different solvents and in the solid state. The IR data of $[\text{M}_2\text{Cp}_2(\text{CO})_3(\text{CNR})]$ ($\text{M} = \text{Ru}$, $\text{R} = 2,6\text{-C}_6\text{H}_3\text{Me}_2 = \text{Xyl}$, **2a-Ru**; $\text{M} = \text{Ru}$, $\text{R} = \text{CH}_2\text{Ph} = \text{Bn}$, **2b-Ru**; $\text{M} = \text{Ru}$, $\text{R} = \text{Me}$, **2c-Ru**; $\text{M} = \text{Fe}$, $\text{R} = \text{Xyl}$, **2a-Fe**; $\text{M} = \text{Fe}$, $\text{R} = \text{Bn}$, **2b-Fe**; $\text{M} = \text{Fe}$, $\text{R} = \text{Me}$, **2c-Fe**) and $[\text{M}_2\text{Cp}_2(\text{CO})_3\{\mu\text{-CNR}(\text{Me})\}]\text{CF}_3\text{SO}_3$ ($\text{M} = \text{Ru}$, $\text{R} = \text{Xyl}$, **4a-Ru**; $\text{M} = \text{Ru}$, $\text{R} = \text{Bn}$, **4b-Ru**; $\text{M} = \text{Ru}$, $\text{R} = \text{Me}$, **4c-Ru**; $\text{M} = \text{Fe}$, $\text{R} = \text{Xyl}$, **4a-Fe**; $\text{M} = \text{Fe}$, $\text{R} = \text{Bn}$, **4b-Fe**; $\text{M} = \text{Fe}$, $\text{R} = \text{Me}$, **4c-Fe**) are comparatively presented, and the back-donation from the dimetallic core to π -acceptor ligands in complexes **4** is discussed. A new synthetic procedure to access **2a-Ru** is reported, affording $[\text{Ru}_2\text{Cp}_2(\text{CO})_2(\text{CNXyl})_2]$ (**3**) as by-product, as well as the single crystal X-ray structures of **2b-Ru** and **4b-Ru**. DFT calculations were carried out to elucidate the relative stability of isomeric forms within the series of isocyanide adducts **2-Ru** and **3**.

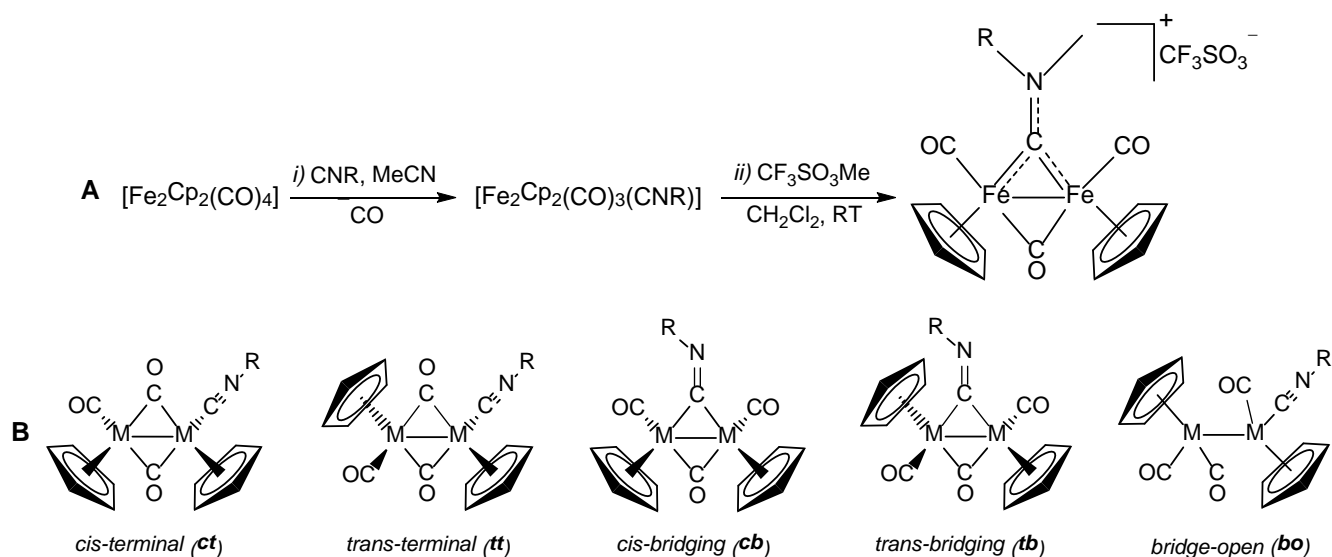
Keywords: diruthenium complexes; diiron complexes; carbonyl ligand; isocyanide ligand; aminocarbyne ligand; 3d and 4d transition metals; π -back-donation

Introduction

In 1975, Chatt, Richards, Pombeiro and co-workers reported the first synthesis of an aminocarbyne species via isocyanide protonation [1], and in the following decades the electrophilic addition to isocyanide ligands became a classical approach to access aminocarbyne complexes of a range of transition metals [2,3,4].

The same route is feasible from the easily available iron(I) dimer $[\text{Fe}_2\text{Cp}_2(\text{CO})_4]$ (**1-Fe**; $\text{Cp} = \eta^5\text{-C}_5\text{H}_5$) and was widely investigated in the last decades of the past century [5]. We recently described an optimized two-step procedure to obtain $[\text{Fe}_2\text{Cp}_2(\text{CO})_2(\mu\text{-CO})\{\mu\text{-CNR}(\text{R}')\}]^+$ complexes ($\text{R}, \text{R}' = \text{alkyl or aryl}$), see Scheme 1A [6, 7, 8]. First, thermal substitution of one carbonyl ligand with isocyanide is performed in acetonitrile using a molar excess of the metal reactant to minimize poly-substitution [7]. The resulting adducts $[\text{Fe}_2\text{Cp}_2(\text{CO})_3(\text{CNR})]$ are obtained as mixtures of cis-trans isomers (with reference to the mutual orientation of the Cp ligands) and terminal-bridging isomers (with reference to the coordination of the isocyanide). The isomeric species usually undergo interconversion in solution at room temperature following the Adams-Cotton mechanism [9], consisting in the formation of bridge-opened structures followed by rotation around the Fe-Fe bond and subsequent bridge-closing [10]. The isomeric composition is variable on changing the isocyanide substituent (R) and the polarity of the solvent, with more polar solvents favoring cis structures (**ct** and **cb** in Scheme 1B, $\text{M} = \text{Fe}$) rather than trans (**tt** and **tb**). DFT calculations highlighted the higher stability provided by the bridging coordination of the isocyanide ligand, although the energy difference with respect to the other isomers is generally rather small. In practice, a mixture of four species is commonly observed, and for instance a relative quantification was performed on $[\text{Fe}_2\text{Cp}_2(\text{CO})_3(\text{CNMe})]$ by a low-temperature NMR study in CD_2Cl_2 solution: 77% (**ct**), 2% (**tt**), 16% (**cb**), 5% (**tb**) [9a]. Kinetic factors may play an important role, and isocyanides with bulky R groups, such as cyclohexyl (Cy) and 2,6-dimethylphenyl (Xyl), are prevalently found in terminal position even at high temperatures, the migration to one bridging site being inhibited [7].

The alkylation of isocyanide belonging to the different $[\text{Fe}_2\text{Cp}_2(\text{CO})_3(\text{CNR})]$ forms converges to a single structure containing a bridging aminocarbyne ligand and, usually, the Cp ligands in cis position, Scheme 1A[8]. Such diiron aminocarbyne complexes represent in turn versatile platforms to build many organometallic architectures [4, 11] with possible biological implications [12].



Scheme 1. A) Two-step synthesis of diiron μ -aminocarbene complexes from $[\text{Fe}_2\text{Cp}_2(\text{CO})_4]$ via isocyanide alkylation (R = alkyl or aryl). B) Possible isomeric forms displayed by mono-isocyanide adducts (M-M = Fe-Fe, Ru-Ru).

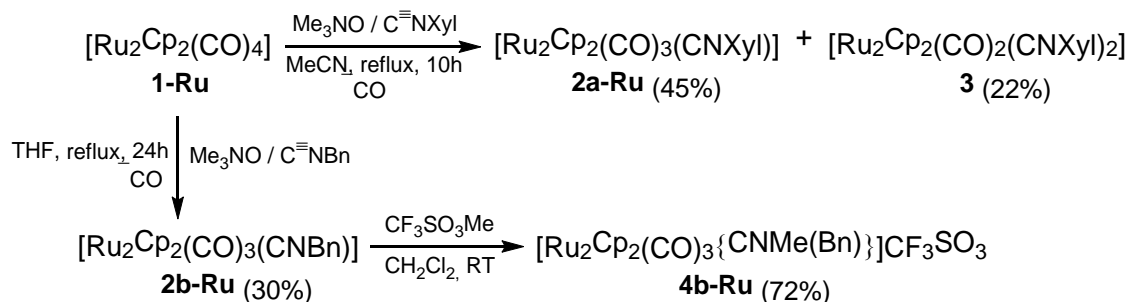
The route depicted in Scheme 1A is viable also for diruthenium complexes, although this piece of chemistry has been considerably less investigated [13]. $[\text{Ru}_2\text{Cp}_2(\text{CO})_4]$ (**1-Ru**) is commercially available and, similarly to $[\text{Fe}_2\text{Cp}_2(\text{CO})_4]$, exists in solution as a mixture of isomers [14]. A few examples of both $[\text{Ru}_2\text{Cp}_2(\text{CO})_3(\text{CNR})]$ and $[\text{Ru}_2\text{Cp}_2(\text{CO})_3\{\mu\text{-CNMe(R)}\}]^+$ (R = Me, PhCH_2 = Bn or 2,6- $\text{C}_6\text{H}_3\text{Me}_2$ = Xyl) derivatives have been reported [15, 16], nevertheless related structural aspects have been barely elucidated. Notably, to the best of our knowledge, crystallographic characterizations on such two classes of compounds are still missing in the literature. Herein, we report and discuss IR, X-ray and DFT results, and trace a comparison between diruthenium complexes and their diiron counterparts.

Results and discussion

First, we revisited some aspects of the structure of **1-Ru** by IR spectroscopy. The isomeric forms displaying either two bridging carbonyl ligands or none (i.e., double bridge, **db**, and bridge-open, **bo**,

respectively, Chart 1) are easily recognized by their IR absorptions, and their relative amount is sensitive to solvent and temperature [14,17]. We recorded IR spectra in a range of solvents, and found that the overall **bo/db** ratio is highly responsive to the solvent polarity, decreasing along the sequence: toluene (0.375D) > CH₂Cl₂ (1.60 D) \approx THF (1.75 D) > MeCN (3.93D) (Figure S1; dipole moments are from reference [18]). By contrast, **1-Fe** shows only a little amount of bridge-open forms in solution, and related IR spectra are much less solvent-dependent (Figure S2) [19]. Interestingly, the pattern of carbonyl absorptions in the solid-state spectra of **1-Ru** and **1-Fe** is very similar, and the lack of bands above 1950 cm⁻¹ suggests the absence of **bo** isomers in the solid (Figure S3).

Complex [Ru₂Cp₂(CO)₃(CNXyl)] (**2a-Ru**) was synthesized by TMNO-induced CO/xylyl isocyanide substitution in refluxing acetonitrile (Scheme 2; TMNO = Me₃NO); **2a-Ru** was then isolated in a moderate yield upon alumina chromatography, beside a lower amount of the disubstituted product **3**. On the other hand, the benzylisocyanide adduct [Ru₂Cp₂(CO)₃(CNBn)] (**2b-Ru**) was best prepared following the literature procedure (refluxing THF; ca. 30% yield) [16]; subsequent methylation afforded in a good yield the μ -aminocarbyne complex **4b-Ru**, which was purified by alumina chromatography (Scheme 2). The spectroscopic characterization of **2a-Ru** is supplied here for the first time.



Scheme 2. Synthesis of diruthenium isocyanide and μ -aminocarbyne complexes from [Ru₂Cp₂(CO)₄]. Xyl = 2,6-C₆H₃Me₂ (meta-xylyl); Bn = CH₂Ph (benzyl).

Crystals of **2b-Ru** and **4b-Ru** suitable for X-ray analysis were collected from dichloromethane/pentane and dichloromethane/hexane mixtures, respectively. The two structures are shown in Figure 1, with

relevant bonding parameters given in Table 1. They are the first examples ever reported for the families of complexes $[\text{Ru}_2\text{Cp}_2(\text{CO})_3(\text{CNR})]$ and $[\text{Ru}_2\text{Cp}_2(\text{CO})_3\{\mu\text{-CNMe(R)}\}]^+$. Compounds **2b-Ru** and **4b-Ru** contain the same *cis*- $[\text{Ru}_2\text{Cp}_2(\text{CO})_2(\mu\text{-CO})]$ core, which is bonded to a bridging $\{\mu\text{-CNBn}\}$ isocyanide ligand in **2b-Ru** and to a bridging $\{\mu\text{-CN(Me)(Bn)}\}^+$ aminocarbyne ligand in **4b-Ru**. All the bridging ligands (i.e., $\mu\text{-CO}$, $\mu\text{-CNBn}$ and $[\mu\text{-CN(Me)(Bn)}]^+$) display an almost perfect symmetrical bonding to the Ru atoms. A shortening of the Ru-C contacts involving the $\mu\text{-CNBn}$ and $[\mu\text{-CN(Me)(Bn)}]^+$ ligands is observed passing from the neutral isocyanide **2b-Ru** [Ru(1)-C(4) 2.038(2) Å, Ru(2)-C(4) 2.059(2) Å] to the cationic aminocarbyne **4b-Ru** [Ru(1)-C(4) 1.981(5) Å, Ru(2)-C(4) 1.999(5) Å]. This feature accounts for the strong π -acceptor character of the bridging aminocarbyne, enhancing $\text{Ru}_2 \rightarrow \text{C}$ back-donation at the expense of the carbyne-N bond (Scheme 3) [4, 20]. Accordingly, the C(4)-N(1) bonding distance is significantly elongated in **4b-Ru** [1.286(7) Å] compared to **2b-Ru** [1.228(3) Å]. In particular, the C(4)-N(1) distance of **4b-Ru** falls in the range [1.28-1.30 Å] for an iminium bond [21], whereas the shorter distance observed in **2b-Ru** is in keeping with a partial triple bond of a bridging isocyanide [22]. The bonding parameters related to the aminocarbyne moiety in **4b-Ru** are comparable to those previously reported for the aminocarbyne acyl complex $[\text{Ru}_2\text{Cp}_2\{\text{C(O)Ph}\}(\text{CO})(\mu\text{-CO})(\mu\text{-CNMe}_2)]$ [23].

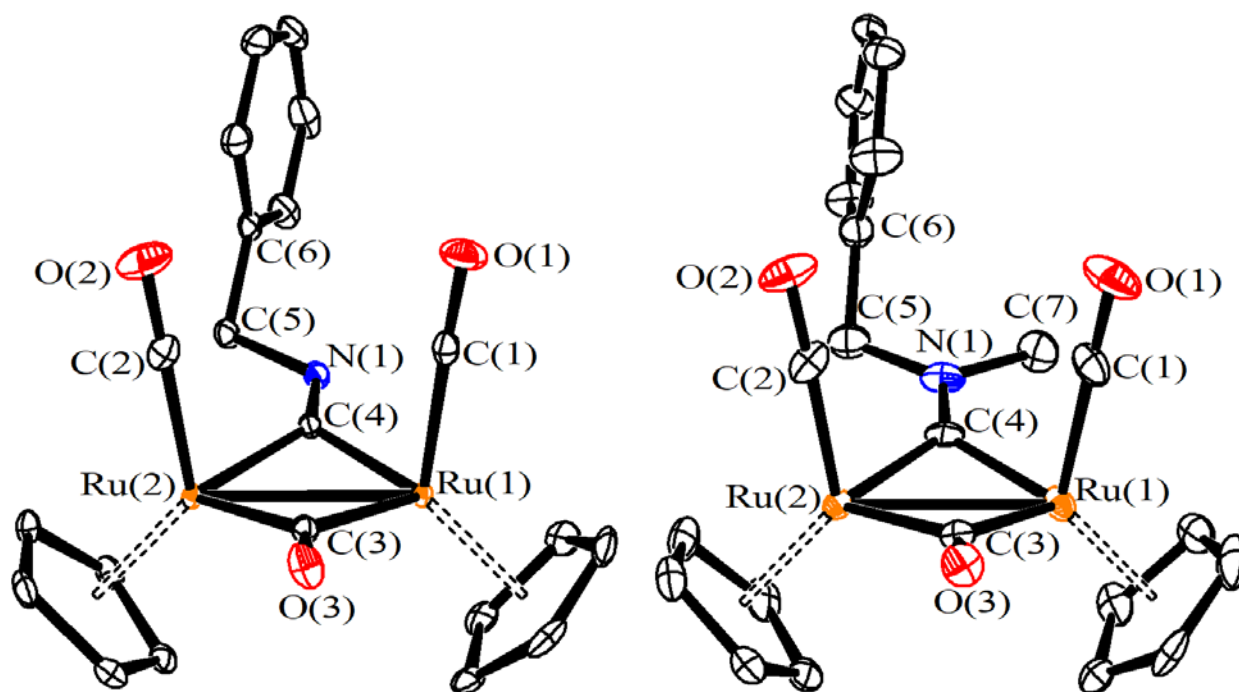
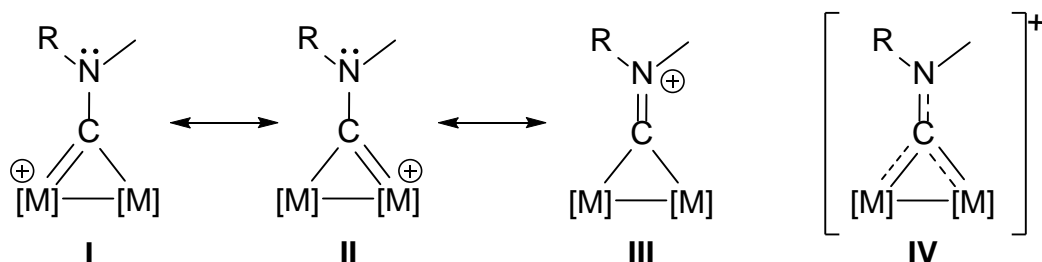


Figure 1. Views of the structures of $[\text{Ru}_2\text{Cp}_2(\text{CO})_3(\text{CNBn})]$ (**2b-Ru**) and of the cation of $[\text{Ru}_2\text{Cp}_2(\text{CO})_3\{\text{CNMe}(\text{Bn})\}]\text{CF}_3\text{SO}_3$ (**4b-Ru**), with labelling. Displacement ellipsoids are at the 50% probability level. H-atoms have been omitted for clarity.

Table 1. Selected bond lengths (Å) and angles (°) for **2b-Ru** and **4b-Ru**.

| | 2b-Ru | 4b-Ru |
|------------------------|--------------|--------------|
| Ru(1)-Ru(2) | 2.7244(2) | 2.7101(6) |
| Ru(1)-Cp _{av} | 2.261(4) | 2.252(13) |
| Ru(2)-Cp _{av} | 2.264(4) | 2.245(13) |
| Ru(1)-C(1) | 1.854(2) | 1.875(6) |
| Ru(2)-C(2) | 1.866(2) | 1.876(5) |
| Ru(1)-C(3) | 2.030(2) | 2.052(5) |
| Ru(2)-C(3) | 2.026(2) | 2.073(5) |
| Ru(1)-C(4) | 2.038(2) | 1.981(5) |
| Ru(2)-C(4) | 2.059(2) | 1.999(5) |
| C(1)-O(1) | 1.149(3) | 1.147(7) |
| C(2)-O(2) | 1.142(3) | 1.135(7) |
| C(3)-O(3) | 1.177(3) | 1.162(6) |
| C(4)-N(1) | 1.228(3) | 1.286(7) |
| C(5)-N(1) | 1.472(3) | 1.465(8) |
| Ru(1)-C(3)-Ru(2) | 84.41(8) | 82.1(2) |
| Ru(1)-C(4)-Ru(2) | 83.37(8) | 85.8(2) |

| | | |
|-----------------|------------|----------|
| Ru(1)-C(1)-O(1) | 178.38(18) | 178.7(6) |
| Ru(2)-C(2)-O(2) | 179.4(2) | 176.9(5) |
| C(4)-N(1)-C(5) | 124.05(18) | 122.8(5) |
| N(1)-C(5)-C(6) | 109.63(16) | 110.8(5) |



Scheme 3. Resonance structures representing the bridging aminocarbyne ligand in diruthenium/diiron complexes. **I** and **II** account for $M_2 \rightarrow C$ back-donation, while **III** is indicative of iminium character ($N \rightarrow C$ donation); **IV**: combined representation with delocalized charge.

The ^1H NMR spectrum of **2a-Ru** in CDCl_3 (Figure S5) displays a single set of narrow resonances, indicating that isomers are fluxional, and the interconverting equilibria are fast in the NMR timescale. Note that also **1-Ru** shows a single, sharp ^1H NMR resonance at 5.28 ppm in CDCl_3 (Figure S4) and, while the spectrum of **1-Fe** resolves in two distinct signals below -50°C (cis/trans isomers), that of **1-Ru** does not reach the slow-exchange limit even at -100°C [14].

On the other hand, as underlined in the Introduction, IR spectroscopy allows to detect the presence of the different isomers, as it operates to a much smaller timescale. Table 2 comparatively shows IR data related to a series of diruthenium isocyanide, $[\text{Ru}_2\text{Cp}_2(\text{CO})_3(\text{CNR})]$ (**2-Ru**), and aminocarbyne complexes, $[\text{Ru}_2\text{Cp}_2(\text{CO})_3\{\text{CNMe(R)}\}]^+$ (**4-Ru**), and their corresponding diiron homologues **2-Fe** and **4-Fe** [23].

Regarding the isocyanide species, IR features indicate a higher tendency for the isocyanide ligand to occupy a bridging coordination site in diruthenium complexes than in the diiron ones. Thus, while the xylylisocyanide ligand in **2a-Fe** is found almost exclusively as terminal [7], in **2a-Ru** a band at 1714 cm^{-1} (CH_2Cl_2 solution) accounts for the presence of forms with bridging coordinated CNXyl .

Moreover, **2b-Fe** exists in CH₂Cl₂ solution as a mixture of terminal/bridging isomers, whereas the benzyliisocyanide in **2b-Ru** has been detected almost exclusively as a bridging ligand in CH₂Cl₂, coherently with the single crystal X-ray diffraction analysis (see above). In this respect, a comparison with the diiron homologue (Figure S6) helps to identify two weak bands (2041, 1745 cm⁻¹) ascribable to isomer(s) with a terminal benzyl isocyanide. In contrast, the solid-state spectra of **2b-Fe** and **2b-Ru** are relatively similar (Figure S7), and the isocyanide-bridging forms are dominant for both.

The aminocarbyne complexes **4** share a common IR pattern consisting of four bands, two of them related to terminal carbonyls, one to bridging carbonyl and one to the carbyne-nitrogen bond. In the diiron complexes, the carbonyl absorptions are 2-6 cm⁻¹ shifted to lower wavenumbers with respect to the corresponding diruthenium species (CH₂Cl₂ solution; Figures S8-S10). The carbyne-nitrogen stretching faces an even higher shift (+ 6-12 cm⁻¹) on going from Fe-Fe to Ru-Ru. Combined, these findings indicate that enhanced back-donation to the carbonyl and aminocarbyne ligands takes place from the diiron(I) core with respect to the diruthenium(I) one (see Scheme 3). A similar trend is hard to be traced for the isocyanide adducts **2**, being IR data related to mixtures of isomers.

The degree of π -back-bonding to π -acceptor ligands within homologous series of complexes belonging to a triad of transition metals was deeply discussed by Basolo [24]. Kinetic studies on the substitution reactions of carbonyl ligands evidenced higher reaction rates for a variety of low-valent 4d metal complexes compared to the corresponding 3d and 5d species. This fact implies that metal-ligand bond strengths may be higher for 3d than 4d metals, as confirmed by BDE (bond dissociation energy) measurements [25]. This is tentatively explained according to the higher degree of π -backdonation from 3d soft metal centers compared to the situation in analogous 4d species, due to the generally lower electronegativity of 3d transition elements with respect to the corresponding 4d ones [26]. Spectroscopic data reflecting the same concept have appeared in the literature, although not fully rationalized [27]. An alternative point of view has been proposed by Wolczanski and coworkers based

on studies of (silox)₃MX_n derivatives (silox = ^tBu₃SiO; M = Nb, Ta, Mo, W) [28]. The greater density of states (DOS) observed for second row transition metal complexes is an important factor in determining a relatively flat transition state, thus ending with their generally faster reactivity compared to the corresponding species of the third transition series [28].

Table2. Comparison of selected IR data for homologous diiron and diruthenium complexes.

| Complex ^[a] | $\bar{\nu}$ (t-CN) / cm ⁻¹ | $\bar{\nu}$ (t-CO) / cm ⁻¹ | $\bar{\nu}$ (μ-CO) / cm ⁻¹ | $\bar{\nu}$ (μ-CN) / cm ⁻¹ | Ref. ^[b] |
|--|---------------------------------------|---------------------------------------|---------------------------------------|---------------------------------------|---------------------------|
| [Ru ₂ Cp ₂ (CO) ₃ (CNXyl)] (2a-Ru) | 2100m | 1997s, 1953s | 1753s | 1714w | <i>this work</i> |
| [Fe ₂ Cp ₂ (CO) ₃ (CNXyl)] (2a-Fe) | 2090s | 1989m, 1950s | 1783w, 1752s | - | [7] |
| [Ru ₂ Cp ₂ (CO) ₃ (CNBn)] (2b-Ru) | 2041w | 1994s, 1952m | 1790m, 1745w | 1705s | <i>this work</i> |
| [Fe ₂ Cp ₂ (CO) ₃ (CNBn)] (2b-Fe) | 2131m | 1989s, 1948s | 1784m, 1747s | 1710m | [7] |
| [Ru ₂ Cp ₂ (CO) ₃ (CNMe)] (2c-Ru) | 2060 | 2003, 1958, 1964 | 1808, 1772 | 1729 | [15] (<i>hexane</i>) |
| [Fe ₂ Cp ₂ (CO) ₃ (CNMe)] (2c-Fe) | 2138, 2116 | 1997, 1957, 1953 | 1801, 1772 | 1734 | [5a] (<i>hexane</i>) |
| | 2153m | 1988m, 1984s | 1778w, 1745s | 1719w | [7] |
| [Ru ₂ Cp ₂ (CO) ₃ {μ-CNMe(Xyl)}]CF ₃ SO ₃ (4a-Ru) | - | 2027s, 1994w | 1846m | 1540w | <i>this work</i> |
| [Fe ₂ Cp ₂ (CO) ₃ {μ-CNMe(Xyl)}]CF ₃ SO ₃ (4a-Fe) | - | 2023s, 1992w | 1840m | 1530w | [12] |
| Δ(Fe→Ru) | | + 5 / + 2 cm ⁻¹ | +6 cm ⁻¹ | + 10 cm ⁻¹ | |
| [Ru ₂ Cp ₂ (CO) ₃ {μ-CNMe(Bn)}]CF ₃ SO ₃ (4b-Ru) | - | 2025s, 1992m | 1841m | 1582w | <i>this work</i> |
| [Fe ₂ Cp ₂ (CO) ₃ {μ-CNMe(Bn)}]CF ₃ SO ₃ (4b-Fe) | - | 2020s, 1989m | 1836m | 1576w | [12] |
| Δ(Fe→Ru) | | +5 / + 3 cm ⁻¹ | + 5 cm ⁻¹ | +6 cm ⁻¹ | |
| [Ru ₂ Cp ₂ (CO) ₃ {μ-CNMe ₂ }]CF ₃ SO ₃ (4c-Ru) | - | 2026s, 1993w | 1840m | 1614w | <i>this work</i> |
| [Fe ₂ Cp ₂ (CO) ₃ {μ-CNMe ₂ }]CF ₃ SO ₃ (4c-Fe) | - | 2022s, 1990w | 1835m | 1602w | [12] |
| Δ(Fe→Ru) | | + 4 / + 3 cm ⁻¹ | + 5 cm ⁻¹ | +12 cm ⁻¹ | |

[a] IR data in CH₂Cl₂ solution, except for [M₂Cp₂(CO)₃(CNMe)] (M = Fe, Ru; hexane solution). Relative intensity reported as strong (s), medium (m), weak (w). [b] Literature reference for the spectral data.

The structures of **2a-Ru** and **2b-Ru** were investigated by DFT to determine the relative stability of the different isomers (Scheme 1). The level of theory is BP86-D3(BJ)/ZORA-tzvp/ZORA and the solvent was considered through the conductor-like polarizable continuum model (dichloromethane). The results are summarized in Table 3, while Table 4 summarized the results previously reported for a series of analogous diiron compounds [7].

Table 3. Relative Gibbs free energies (in kcal/mol) of the different isomers of **2a-Ru** and **2b-Ru** (CH₂Cl₂ solution).

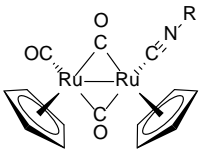
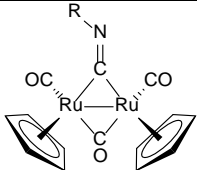
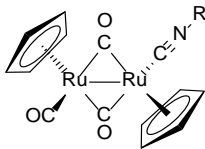
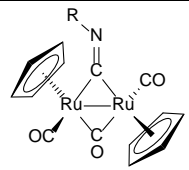
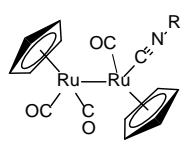
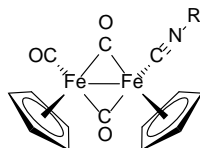
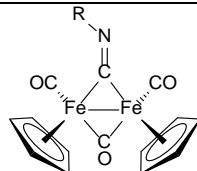
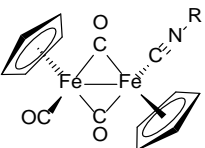
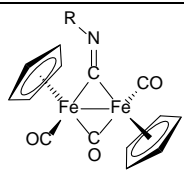
| |  |  |  |  |  |
|---------------------------|---|---|--|---|---|
| | ct | cb | tt | tb | bo |
| 2a-Ru (R = Xyl) | 1.6 | 0.0 | 2.6 | 0.0 | 9.3 |
| 2b-Ru (R = Bn) | 4.4 | 0.1 | 4.8 | 0.0 | 11.6 |

Table 4. Relative enthalpies of the isomers predictable for diiron isocyanide complexes [7].

| |  |  |  |  |
|---|---|---|---|---|
| | ct | cb | tt | tb |
| R | | | | |
| 1H-indol-6-yl | 1.6 | 0.0 | 2.6 | 0.0 |
| CH ₂ PO ₃ Et ₂ | 4.4 | 0.1 | 4.8 | 0.0 |
| C ₆ H ₁₁ | 4.4 | 0.1 | 4.8 | 0.0 |
| 4-C ₆ H ₄ OMe | 4.4 | 0.1 | 4.8 | 0.0 |
| Xyl | 4.4 | 0.1 | 4.8 | 0.0 |
| Me | 4.4 | 0.1 | 4.8 | 0.0 |
| 1H-indol-6-yl | 4.4 | 0.1 | 4.8 | 0.0 |
| CH ₂ PO ₃ Et ₂ | 4.4 | 0.1 | 4.8 | 0.0 |

For both complexes **2a-Ru** and **2b-Ru**, the most stable isomers are **cb** and **tb**, being practically isoenergetic in solution. Note that the situation is slightly different in the gas-phase, *e.g.* **2a-Ru-cb** is less stable than **2a-Ru-tb** by 0.9 kcal/mol, coherently with the common higher stability of *trans* isomers in nonpolar media. Isomers bearing a terminal isocyanide are sensibly less stable, but **2a-Ru-ct** is accessible ($\Delta G = 1.6$ kcal/mol), in agreement with the experimental detection of the corresponding IR peak (2100 cm⁻¹, see Table 2). For **2b-Ru**, isomers bearing a terminal isocyanide are less stable (relative $G \geq 2.4$ kcal/mol), justifying the very low intensity of the corresponding absorption in the IR spectrum. Calculated bonding parameters for **2b-Ru-cb** (see Table S1) substantially agree with the experimental X-ray data; a view of the DFT-calculated structure of **2a-Ru-cb** is shown in Figure 2.

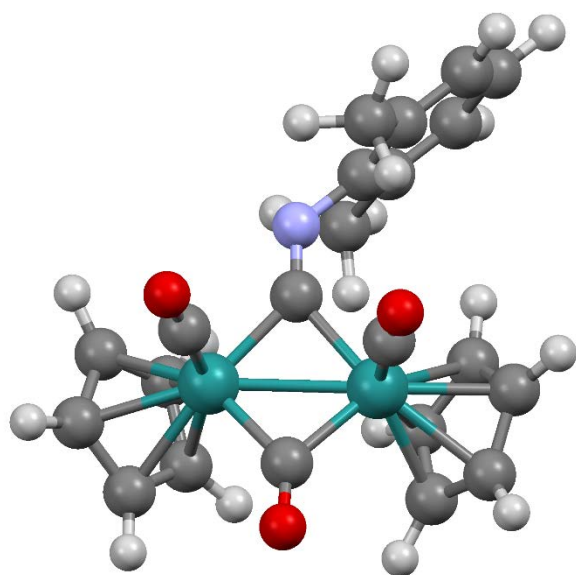


Figure 2. DFT-optimized structure of the most stable isomer of **2a-Ru**, i.e. **2a-Ru-cb**. Relevant distances (Å) and angles (°): Ru-Ru 2.726; Ru-C_{terminal CO}, av 1.858; C-O_{terminal CO}, av 1.164; Ru-C_{bridging CO}, av 2.046; C-O_{bridging CO} 1.187; C_{bridging aminocarbyne}-N 1.241; Ru-C_{bridging CO}-Ru 83.6; Ru1-C_{bridging aminocarbyne}-Ru2 83.7.

In contrast to **2a-Ru**, we previously found that **2a-Fe** is generated from **1-Fe** almost exclusively as a mixture of terminal-CNXyl adducts (**ct** + **tt**), despite DFT calculations highlighted the higher stability of bridging-CNXyl structures. This fact was explained invoking the steric hindrance associated to the xyl group, kinetically favoring its terminal coordination and blocking the isomerization mechanism (see Introduction) [7]. Thermal treatment was partially effective to enable terminal to bridging migration of the xylisocyanide. It is possible that the experimental observation of bridging-CNXyl species in the case of **2a-Ru** is because **2a-Ru-bo**, which is a reasonable intermediate for all the isomerization processes, is relatively more stable compared to the corresponding iron species, leading to lower activation barriers. This hypothesis is supported by the behavior of **1-Ru** versus **1-Fe** in solution (*vide supra*). On the other hand, it is interesting to note how the CO/isocyanide replacement in

1-Ru destabilizes the open-bridge forms, which are accessible as intermediates for $[\text{Ru}_2\text{Cp}_2(\text{CO})_3(\text{CNR})]$ but not detected in solution [15].

The structures and salient geometric parameters of **2a-Ru-bo** and **2b-Ru-bo** are supplied in the Supporting Information (Table S1, Figure S11). The bond order of the Ru-Ru bond, falling between 0.43 and 0.55 for all the isomers containing bridging ligands, increases up to 0.75 and 0.64 for **2a-Ru-bo** and **2b-Ru-bo**, respectively. This is not reflected in a reduced Ru-Ru distance (2.805 Å).

A DFT study was then carried out to ascertain structural aspects on the unprecedented di-isocyanide adduct **3** (Table S1, Figure S12). The structure with two bridging isocyanide ligands resulted the most stable one (**3-cbb**). The IR spectrum of **3** displays C-N stretches corresponding to terminal (2076 cm^{-1}) and bridging (1679 cm^{-1}) isocyanide ligands, being indicative of the presence of isomers **3-cbb** and **3-bo**, in agreement with DFT calculations. Indeed, the open geometry **3-bo** is particularly stable in this case (+1.6 kcal/mol with respect to **3-cbb**), likely because of the two CH- π interactions between the Cp moieties and the aromatic ring of the isocyanide ligands. The structures of **3-cbb** and **3-bo** are shown in Figure 3. The Ru-Ru bond is 2.809 Å long, and the bond order (0.83) is higher than in **2a-Ru-bo** (0.75). Note that the terminal/bridging-isocyanide forms, **3-tb**, resulted much less stable (+3.5 and +3.9 kcal/mol for *trans* and *cis* isomers, respectively). Once again, the diiron counterparts behave differently, with $[\text{Fe}_2\text{Cp}_2(\text{CO})(\text{CNR})(\mu\text{-CO})(\mu\text{-CNR})]$ being detected in solution, together with $[\text{Fe}_2\text{Cp}_2(\text{CO})_2(\mu\text{-CNR})_2]$ (R = Me, *t*Bu, Ph, 4-C₆H₄Me) [29].

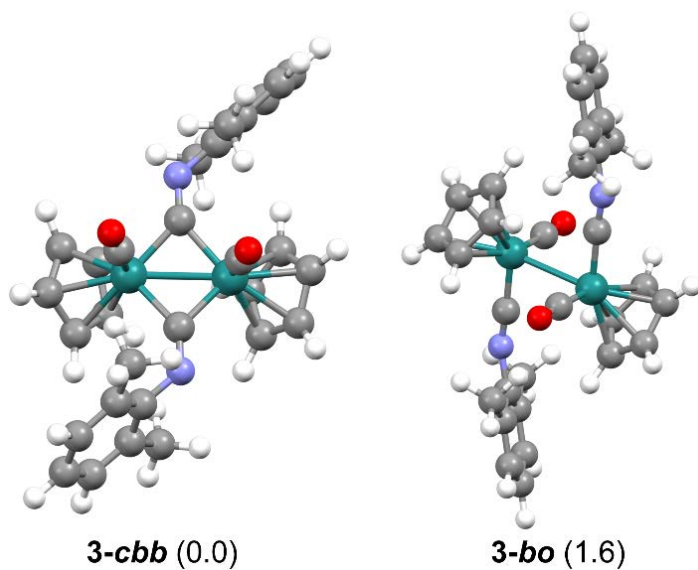


Figure 3. Views of DFT-optimized structures and relative free Gibbs energies, in kcal/mol, of experimentally observed isomers of **3**.

The calculated structure of **4b-Ru** is shown in Figure 4, with relevant bond distances and angles in the caption, evidencing a good correlation with the experimental X-ray data. The bond orders evidence that the μ -CN bond is perfectly halfway between single and double (Mayer bond order, b.o.: 1.50): this aminocarbyne-iminium hybrid structure resembles the situation in analogous diiron complexes (see Scheme 3) [12b].

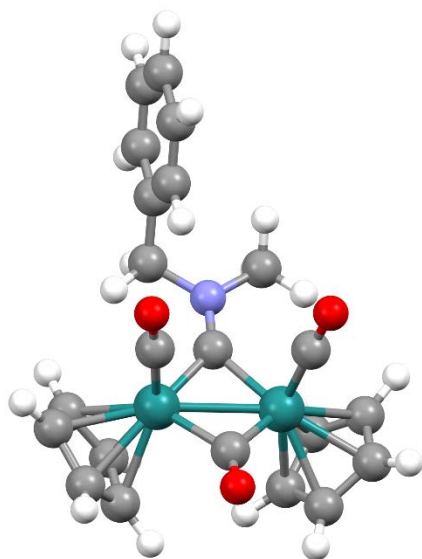


Figure 4. DFT-optimized structure of **4b-Ru**. Main bond distances (Å) and angles (°): Ru-Ru 2.728; Ru-C_{terminal} CO, av 1.878; C-O_{terminal} CO, av 1.157; Ru-C_{bridging} CO, av 2.063; C-O_{bridging} CO 1.178; C_{bridging} aminocarbyne-N 1.301; Ru-C_{bridging} CO-Ru 82.7; Ru1-C_{bridging} aminocarbyne -Ru2 86.2.

Conclusions

The synthesis of bridging aminocarbyne complexes from the diiron bis-cyclopentadienyl species $[\text{Fe}_2\text{Cp}_2(\text{CO})_4]$ via the intermediacy of isocyanide adducts is well documented in the literature, otherwise the parallel diruthenium chemistry has been much less investigated. Here, we describe a multi-technique study to elucidate synthetic, structural and thermodynamic aspects concerning selected diruthenium isocyanide and aminocarbyne complexes, including the very first X-ray characterizations of compounds belonging to these two families. In general, the results evidence negligible or small differences with respect to the diiron homologues, however IR data are sufficiently sensitive to outline a slight but significant decrease of back-donation from the dimetallic core to π -acceptor ligands (carbonyls, aminocarbyne) on going from diiron to diruthenium cationic complexes. In contrast to the general observation that metal-ligand bond strengths increase on descending a transition metal triad, the lower bond energies involving 4d metals and π -acceptor ligands was previously recognized and, in a

limited number of cases, tentatively explained based on the correlation between electronegativity values and back-donation. The comparative IR data here reported on homologous 3d and 4d metal complexes constitute a further, clear experimental support to that phenomenon.

Experimental

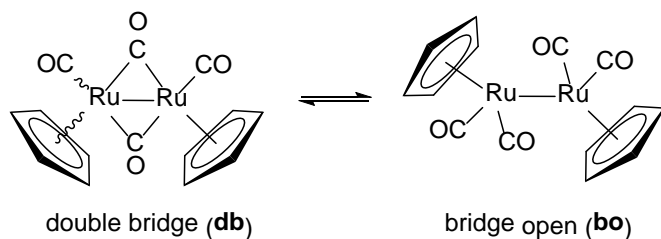
1. General experimental details.

[Ru₂Cp₂(CO)₄], **1-Ru** (carbon 36.4-38.9%), was purchased from Merck, other reactants and solvents were obtained from Merck or TCI Chemicals and were of the highest purity available. Complexes **2b-Ru** [16], **4a-Ru** [23] and **4c-Ru** [23] were prepared according to the indicated literature procedure. NMR spectra were recorded at 298 K on a Bruker Avance II DRX400 instrument equipped with a BBFO broadband probe. CDCl₃ stored in the dark over 3 Å MS was used for NMR analysis. Chemical shifts are referenced to the residual solvent peaks (¹H, ¹³C) [30]. IR spectra of solid samples (650-4000 cm⁻¹) were recorded at 298 K on a Perkin Elmer Spectrum One FT-IR spectrometer, equipped with a UATR sampling accessory. IR spectra of solutions were recorded using a CaF₂ liquid transmission cell (1500–2300 cm⁻¹) on a Perkin Elmer Spectrum 100 FT-IR spectrometer. IR bands and ¹³C NMR resonances attributed to terminal and bridging CO/CNR ligands are indicated as t-CO/t-CN and μ-CO/μ-CN, respectively. IR spectra were processed with Spectragryph software [31].

2. Synthesis and/or characterization of diruthenium compounds.

[Ru₂Cp₂(CO)₄] (Chart 1).

Chart 1. Structures of [Ru₂Cp₂(CO)₄] (**1-Ru**; wavy bonds represent *cis/trans* isomerism).

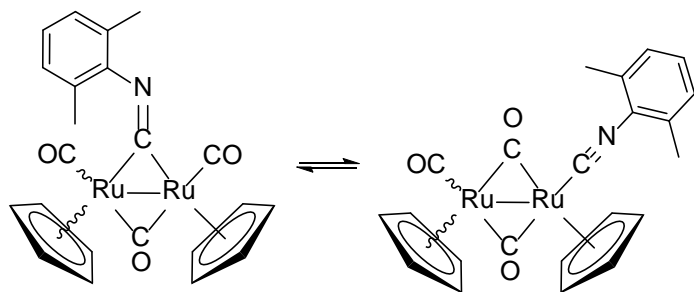


IR (solid state): $\tilde{\nu}/\text{cm}^{-1}$ = 3896w, 3546w, 3115w, 3091w, 2485w, 1933s-br (CO), 1913s-sh (CO), 1757s-br (μ-CO), 1735s-sh (μ-CO), 1677m-sh, 1427m, 1410m, 1345m, 1107w, 1054w, 1010m, 993m, 923w, 913w, 854w, 833m, 810s, 687m. IR (CH₂Cl₂): $\tilde{\nu}/\text{cm}^{-1}$ = \approx 2008m-sh (t-CO, **bo**), 2001s (t-CO,

db), 1964-1960s (t-CO, **bo**+ **db**), 1935m-sh (t-CO, **bo**), 1772s (μ -CO, **db**) cm^{-1} . IR (MeCN): $\tilde{\nu}/\text{cm}^{-1}$ = 2005m-sh (t-CO, **bo**), 1995s (t-CO, **db**), 1956m-br (t-CO, **db**), 1934w-sh (t-CO, **bo**), 1774s (μ -CO, **db**) cm^{-1} . IR (THF): $\tilde{\nu}/\text{cm}^{-1}$ = 2008m-sh (t-CO, **bo**), 1996s (t-CO, **db**), 1965m (t-CO, **bo**), 1954m (t-CO, **db**), 1936m (t-CO, **bo**), 1782s (μ -CO, **db**) cm^{-1} . IR (toluene): $\tilde{\nu}/\text{cm}^{-1}$ = 2012m-sh (t-CO, **bo**), 2001s (t-CO, **db**), 1966s (t-CO, **bo**), 1957s-sh (t-CO, **db**), 1936s (t-CO, **bo**), 1783 (μ -CO, **db**). ^1H NMR (CDCl_3): δ/ppm = 5.28 (s).

[Ru₂Cp₂(CO)₃(CNXyl)], 2a-Ru (Chart 2).

Chart 2. Structures of **2a-Ru** (wavy bonds represent *cis/trans* isomerism).

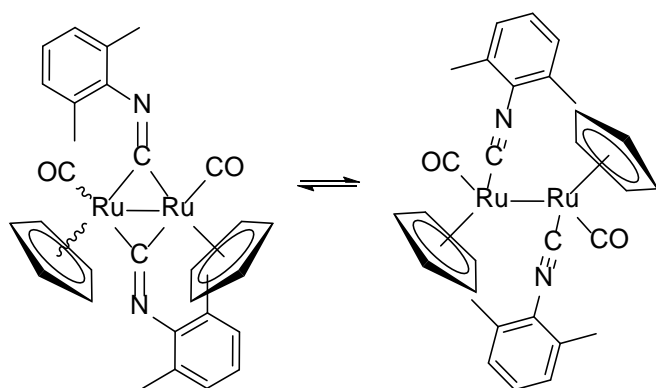


A mixture of [Ru₂Cp₂(CO)₄] (1.86 g, 4.19 mmol), 2,6-dimethylphenylisocyanide (CNXyl; 0.561 g, 4.28 mmol) and Me₃NO (0.600 g, 8.00 mmol) in CH₃CN (30 mL) was refluxed for 10 hours, monitoring its advancement via IR spectroscopy. Then, volatiles were moved under vacuum, the residue was dissolved in the minimum volume of CH₂Cl₂ and the solution was filtered through a short alumina column to remove all solid impurities. Hence, the filtrate was concentrated under reduced pressure and chromatographed on alumina. A first fraction corresponding to unreacted [Ru₂Cp₂(CO)₄] (0.500 g, 1.13 mmol) was isolated using petroleum ether/CH₂Cl₂ (1:1 v/v) as eluent. Elution with neat CH₂Cl₂ allowed to separate the title compound **2a-Ru**. Yellow-orange solid, yield 1.02 g, 1.87 mmol, 45 %. Anal. calcd. for C₂₂H₁₉NO₃Ru₂: C, 48.26; H, 3.50; N, 2.56. Found: C, 48.41; H, 3.39; N, 2.37. IR (CH₂Cl₂): $\tilde{\nu}/\text{cm}^{-1}$ = 2100m-s (t-CN), 1997vs (t-CO), 1953vs (t-CO), 1753s (μ -CO), 1714m (μ -CN). ^1H

NMR (CDCl₃): δ/ppm = 7.06–7.02 (m, 2H, C₆H₃), 7.00–6.94 (m, 1H, C₆H₃); 5.23 (s, 10 H, Cp); 2.31 (s, 6H, CCH₃).

[Ru₂Cp₂(CO)₂(CNXyl)₂], **3 (Chart 3).**

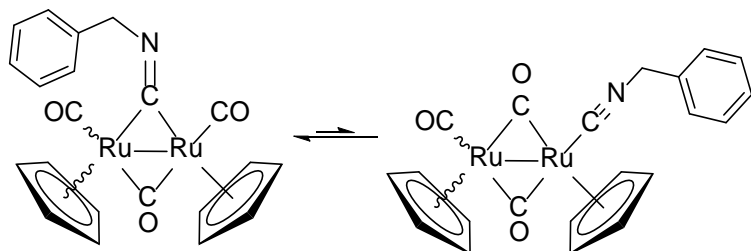
Chart 3. Structures of **3** (wavy bonds represent *cis/trans* isomerism).



The title compound was obtained as a second yellow band from the chromatography of the [Ru₂Cp₂(CO)₄]/CNXyl reaction described above. Yellow-orange solid, yield 0.600 g (22%). Anal. calcd. for C₃₀H₂₈N₂O₂Ru₂: C, 55.37; H, 4.38; N, 4.31. Found: C, 55.21; H, 4.44; N, 4.28. IR (CH₂Cl₂): $\tilde{\nu}/\text{cm}^{-1}$ = 2076s (t-CN), 1990vs (t-CO), 1948vs (t-CO), 1751m (μ -CO), 1679vs (μ -CN). ¹H NMR (CDCl₃): δ/ppm = 7.10-6.80 (m, 6 H, arom); 5.14 (s, 10 H, Cp); 2.28 (s, 12 H, C₆H₃Me₂).

[Ru₂Cp₂(CO)₃(CNBn)], **2b-Ru (Chart 4).**

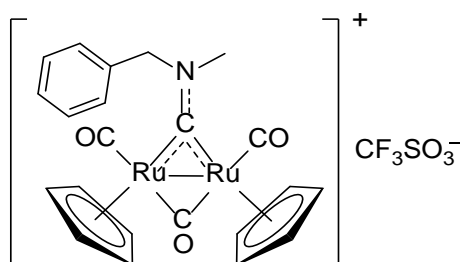
Chart 4. Structures of **2b-Ru** (wavy bonds represent *cis/trans* isomerism).



Prepared as described in the literature from $[\text{Ru}_2\text{Cp}_2(\text{CO})_4]$ (100 mg, 0.23 mmol), Me_3NO (11 mg, 0.15 mmol) and benzyl isocyanide (18 μL , 0.15 mmol)[16]. X-ray quality crystals of **2b-Ru** were obtained from a CH_2Cl_2 solution layered with pentane and settled aside at -20°C . IR (CH_2Cl_2): $\tilde{\nu}/\text{cm}^{-1} = 1995\text{vs}$ (t-CO), 1953m (t-CO), 1791s (μ -CO), 1705s (μ -CN). IR (CH_2Cl_2): $\tilde{\nu}/\text{cm}^{-1} = 2141\text{w}$ (t-CN), 1994s (t-CO), 1952m (t-CO), 1790m (μ -CO), 1745w (μ -CO), 1705s (μ -CN). IR (solid state): $\tilde{\nu}/\text{cm}^{-1} = 3116\text{w}$, 3095w, 3058w, 3028w, 2928w, 2891w, 2835w, 1974s (t-CO), 1934s (t-CO), 1901m-sh, 1772s (μ -CO), 1690s-br (μ -CN), 1493m, 1453m, 1441m, 1411m, 1351w, 1309m, 1106w, 1078w, 1068w, 1055m, 1027w, 999m, 959m, 943w, 912m, 857w, 832m-sh, 818s-sh, 803s, 754s, 736w, 700s, 679s. ^1H NMR (CDCl_3): $\delta/\text{ppm} = 7.41\text{-}7.5$ (m, 5 H, Ph); 5.33 (s, 10 H, Cp); 4.82 (s, 2 H, NCH_2).

$[\text{Ru}_2\text{Cp}_2(\text{CO})_3\{\text{CNMe}(\text{Bn})\}]$, 4b-Ru (Chart 5).

Chart 5. Structure of **4b-Ru**.



Prepared as described in the literature from **2b-Ru** and methyl triflate [16]. X-ray quality crystals of **4b-Ru** were obtained from a CH_2Cl_2 solution layered with *n*-hexane and settled aside at -20°C . IR (CH_2Cl_2): $\tilde{\nu}/\text{cm}^{-1} = 2025\text{s}$ (t-CO), 1992m (t-CO), 1841m (μ -CO), 1595m, 1582w (μ -CN). ^1H NMR (CDCl_3): $\delta/\text{ppm} = 7.45\text{-}7.36$ (m, 5 H, Ph); 5.72, 5.71 (s, 10 H, Cp); 5.66, 5.56 (d, $^2J_{\text{HH}} = 15$ Hz, 2 H, NCH_2); 3.83 (s, 3 H, NCH_3).

3. X-ray crystallography.

Crystal data and collection details for **2b-Ru** and **4b-Ru** are reported in Table 5. Data were recorded on a Bruker APEX II diffractometer equipped with a PHOTON100 detector using Mo–K α radiation. Data were corrected for Lorentz polarization and absorption effects (empirical absorption correction SADABS) [32]. The structures were solved by direct methods and refined by full-matrix least-squares based on all data using F^2 [33]. Hydrogen atoms were fixed at calculated positions and refined by a riding model. All non-hydrogen atoms were refined with anisotropic displacement parameters.

Table 5. Crystal data and measurement details for **2b-Ru** and **4b-Ru**.

| | 2b-Ru | 4b-Ru |
|--|---|--|
| Formula | C ₂₁ H ₁₇ NO ₃ Ru ₂ | C ₂₃ H ₂₀ F ₃ NO ₆ Ru ₂ S |
| FW | 533.49 | 697.60 |
| T, K | 100(2) | 100(2) |
| λ , Å | 0.71073 | 0.71073 |
| Crystal system | Monoclinic | Orthorhombic |
| Space group | $P2_1/n$ | $Pbca$ |
| a , Å | 12.8597(4) | 12.2150(5) |
| b , Å | 11.5823(4) | 19.0901(7) |
| c , Å | 13.2864(4) | 20.7062(8) |
| β , ° | 107.5300(10) | 90 |
| Cell Volume, Å ³ | 1887.04(10) | 4828.4(3) |
| Z | 4 | 8 |
| D_c , g·cm ⁻³ | 1.878 | 1.919 |
| μ , mm ⁻¹ | 1.621 | 1.401 |
| F(000) | 1048 | 2752 |
| Crystal size, mm | 0.24×0.21×0.18 | 0.24×0.19×0.13 |
| θ limits, ° | 1.932–25.998 | 1.967–25.091 |
| Reflections collected | 25860 | 61137 |
| Independent reflections | 3701 [$R_{int} = 0.0263$] | 4302 [$R_{int} = 0.0404$] |
| Data / restraints / parameters | 3701 / 0 / 244 | 4302 / 0 / 326 |
| Goodness on fit on F^2 | 1.185 | 1.371 |
| R_1 ($I > 2\sigma(I)$) | 0.0183 | 0.0414 |
| wR_2 (all data) | 0.0437 | 0.0919 |
| Largest diff. peak and hole, e Å ⁻³ | 0.389 / –0.470 | 1.481 / –1.211 |

4. DFT calculations

All geometries were optimized with ORCA 4.0.1.2 [34], using the BP86 functional with the zero-order regular approximation (ZORA) [35] to take relativistic effects into account and in conjunction with a triple- ζ quality basis set (ZORA-TZVP) and SARC/J auxiliary basis [36]. For ruthenium, the basis set “old-ZORA-TZVP” has been used. The dispersion corrections were introduced using the Grimme D3-parametrized correction and the Becke Johnson damping to the DFT energy [37]. Most of the structures were confirmed to be local energy minima (no imaginary frequencies), but in some cases a small, unavoidable negative frequency relative to the Cp rotation around the M-Cp axis was observed. The solvent was considered through the continuum-like polarizable continuum model (C-PCM, dichloromethane).

Acknowledgements

We gratefully thank the University of Pisa (Fondi di Ateneo 2020) for financial support.

Supporting Information Available

IR spectra, DFT geometries. CCDC reference numbers 2120118 (**2b-Ru**) and 2120119 (**4b-Ru**) contain the supplementary crystallographic data for the X-ray studies reported in this paper. This data can be obtained free of charge at <https://www.ccdc.cam.ac.uk/structures/>. Cartesian coordinates of the DFT-optimized structures are collected in a separated .xyz file.

References

-
- [1] J. Chatt, A. J. L. Pombeiro, R. L. Richards, G. H. D. Royston, K. W. Muir, R. Walker, J. Chem. Soc. Chem. Commun. (1975) 708-709.
- [2] A. J. L. Pombeiro, M. F. C. Guedes da Silva, R. A. Michelin, Coord. Chem. Rev. 218 (2001) 43–74.
- [3] A. J. L. Pombeiro, M. F. C. Guedes da Silva, J. Organomet. Chem. 617-618 (2001) 65-69.
- [4] L. Biancalana, F. Marchetti, Coord. Chem. Rev. 449 (2021) 214203.
- [5] (a) J. Bellerby, M. J. Boylan, M. Ennis, A. R. Manning, J. Chem. Soc. Dalton Trans. (1978) 1185-1189.
- (b) M. Ennis, R. Kumar, A. R. Manning, J. A. S. Howell, P. Mathur, A. J. Rowan, F. S. Stephens, J. Chem. Soc. Dalton Trans. (1981) 1251-1259.
- (c) G. McNally, P. T. Murray, A. R. Manning, J. Organomet. Chem. 243 (1983) C87-C88.
- (d) N. J. Coville, M. O. Albers, E. Singleton, J. Chem. Soc. Dalton Trans. (1982) 1389-1391.
- (e) S. Nakanishi, Y. Taniki, Y. Otsuji, J. Chem. Soc. Chem. Commun. (1993) 709-710.
- [6] R. Mazzoni, F. Marchetti, A. Cingolani, V. Zanotti, Inorganics 7 (2019) 25-43.
- [7] L. Biancalana, G. Ciancaleoni, S. Zacchini, G. Pampaloni, F. Marchetti, Inorg. Chim. Acta, 517 (2021) 120181.
- [8] G. Agonigi, M. Bortoluzzi, F. Marchetti, G. Pampaloni, S. Zacchini, V. Zanotti, Eur. J. Inorg. Chem. (2018) 960–971.
- [9] (a) M. A. Guillevis, E. L. Hancox, B. E. Mann, J. Chem. Soc. Dalton Trans. (1992) 1729-1733.
- (b) R. D. Adams, F. A. Cotton, Inorg. Chem. 13 (1974) 257-262.
- [10] L. J. Farrugia, J. Chem. Soc., Dalton Trans. (1997) 1783-1792.
- [11] F. Marchetti, Eur. J. Inorg. Chem. (2018) 3987-4003.
- [12] (a) D. Rocco, L. K. Batchelor, G. Agonigi, S. Braccini, F. Chiellini, S. Schoch, T. Biver, T. Funaioli, S. Zacchini, L. Biancalana, M. Ruggeri, G. Pampaloni, P. J. Dyson, F. Marchetti, Chem. Eur. J. 2019, 25, 14801 – 14816.

This item was downloaded from IRIS Università di Bologna (<https://cris.unibo.it/>)

When citing, please refer to the published version.

-
- (b) L. Biancalana, M. De Franco, G. Ciancaleoni, S. Zacchini, G. Pampaloni, V. Gandin, F. Marchetti, *Chem. Eur. J.* 2021, 27, 10169–10185.
- [13] (a) L. Busetto, F. Marchetti, S. Zacchini, V. Zanutti, *J. Organomet. Chem.* 691 (2006) 2424–2439.
(b) L. Busetto, F. Marchetti, S. Zacchini, V. Zanutti, *Eur. J. Inorg. Chem.* (2004) 1494-1504.
- [14] J. G. Bullitt, F. A. Cotton, T. J. Marks, *Inorg. Chem.* 11 (1972) 671-676.
- [15] J. A. S. Howell, A. J. Rowan, *J. Chem. Soc. Dalton Trans.* (1980) 503-510.
- [16] L. Busetto, L. Carlucci, V. Zanutti, V. G. Albano, M. Monari, *J. Organomet. Chem.* 447 (1993) 271-275.
- [17] (a) P. McArdle, A. R. Manning, *J. Chem. Soc. A* (1970) 2128-2132.(b) F. A. Cotton, G. Yagupsky, *Inorg. Chem.* 6 (1967), 15-20.
- [¹⁸] CRC Handbook of Chemistry and Physics, 97th ed.; W. M. Heynes Ed.; CRC Press: Boca Raton, FL, 2017.
- [19] A. R. Manning, *J. Chem. Soc. A* 1968, 1319-1324.
- [20] (a) A.J.L. Pombeiro, *J. Organomet. Chem.* 690 (2005) 6021–6040.
(b) A.I.F. Venâncio, M.F.C. Guedes da Silva, L.M.D.R.S. Martins, J. J. R. Frausto da Silva, A.J.L. Pombeiro, *Organometallics* 24 (2005) 4654–4665.
- [21] (a) V.G. Albano, L. Busetto, C. Castellari, M. Monari, A. Palazzi, V. Zanutti, *J. Chem. Soc. Dalton Trans.* (1993) 3661.
(b) P. Bladon, M. Dekker, G.R. Knox, D. Willison, G.A. Jaffari, R.J. Doedens, K.W. Muir, *Organometallics* 12 (1993) 1725
- [22] (a) H. Chikamori, T. Takao, *Organometallics* 38 (2019) 2705.
(b) J. L. Bear, W.-Z. Chen, B. Han, S. Huang, L.-L. Wang, A. Thuriere, E. Van Caemelbecke, K. M. Kadish, T. Ren, *Inorg. Chem.* 42 (2003) 6230.
(c) T. Takao, S. Horikoshi, T. Kawashima, S. Asano, Y. Takahashi, A. Sawano, H. Suzuki, *Organometallics* 37 (2018) 1598.
(d) S. Takemoto, S. Oshio, T. Kobayashi, H. Matsuzaka, M. Hoshi, H. Okimura, M. Yamashita, H. Miyasaka, T. Ishii, M. Yamashita, *Organometallics* 23 (2004) 3587.

This item was downloaded from IRIS Università di Bologna (<https://cris.unibo.it/>)

When citing, please refer to the published version.

-
- (e) T. Takao, N. Obayashi, B. Zhao, K. Akiyoshi, H. Omori, H. Suzuki, *Organometallics* 30 (2011) 5057.
- (f) A. Tahara, M. Kajigaya, T. Takao, H. Suzuki, *Organometallics* 32 (2013) 30.
- [23] V. G. Albano, L. Busetto, C. Camiletti, M. Monari, V. Zanotti, *J. Organomet. Chem.* 563 (1998) 153-159.
- [24] F. Basolo, *Polyhedron* 9 (1990) 1503-1535.
- [25] (a) A. W. Ehlers, Y. Ruiz-Morales, E. Jan Baerends, T. Ziegler, *Inorg. Chem.* 1997, 36, 5031 – 5036.
(b) A. K. Hughes, K. Wade, *Coord. Chem. Rev.* 197 (2000) 191–229.
- [26] S. A. Decker, M. Klobukowski, *J. Am. Chem. Soc.* 1998, 120, 9342 – 9355.
- [27] (a) J. Fajardo, Jr., J. C. Peters, *J. Am. Chem. Soc.* 139 (2017) 16105–16108. (b) X. Xie, Y. Chen, D. Ma, *J. Am. Chem. Soc.* 128 (2006) 16050–16051.
- [28] (a) P. T. Wolczanski, *Chem. Commun.* (2009) 740-757.
(b) K. F. Hirsekorn, E. B. Hulley, P. T. Wolczanski, T. R. Cundari, *J. Am. Chem. Soc.* 130 (2008) 1183-1196.
(c) D. S. Kuiper, R. E. Douthwaite, A.-R. Mayol, P. T. Wolczanski, E. B. Lobkowski, T. R. Cundari, O. P. Lam, K. Meyer, *Inorg. Chem.* 47 (2008) 7139-7153.
- [²⁹] (a) R. D. Adams, F. A. Cotton, *Inorg. Chem.* 13 (1974), 249-253. (b) J. A. Howell, P. Mathur, *J. Organomet. Chem.*, 174 (1979), 335-341. (c) A. R Manning, G. McNally, P. Soye, *Inorg. Chim. Acta*, 180 (1991) 103-110.
- [30] G. R. Fulmer, A. J. M. Miller, N. H. Sherden, H. E. Gottlieb, A. Nudelman, B. M. Stoltz, J. E. Bercaw, K. I. Goldberg, *Organometallics* 29 (2010) 2176-2179.
- [31] F. Menges, "Spectragryph - optical spectroscopy software", Version 1.2.16d @ (2016-2020) <http://www.ffmpeg2.de/spectragryph>.
- [32] G. M. Sheldrick, SADABS-2008/1 - Bruker AXS Area Detector Scaling and Absorption Correction, Bruker AXS: Madison, Wisconsin, USA (2008).
- [33] G. M. Sheldrick, *Acta Crystallogr. C* 71 (2015) 3.
- [34] F. Neese, *Wiley Interdiscip. Rev.: Comput. Mol. Sci.* 8 (2017) e1327.
- [35] C. van Wuelen *J. Chem. Phys.* 109 (1998) 392-399

This item was downloaded from IRIS Università di Bologna (<https://cris.unibo.it/>)

When citing, please refer to the published version.

-
- [36] F. Weigend, Phys. Chem. Chem. Phys. 8 (2006) 1057.
- [37] S. Grimme, J. Antony, S. Ehrlich, H. Krieg, J. Chem. Phys. 132 (2010) 154104.

This item was downloaded from IRIS Università di Bologna (<https://cris.unibo.it/>)

When citing, please refer to the published version.